

Perceive and Calibrate: Analyzing and Enhancing Robustness of Medical Multi-Modal Large Language Models

Dunyuan XU^{1*}, Xikai Yang^{1*,†}, Yaoqian Li¹, Juzheng Miao¹, Jinpeng Li¹ , Pheng-Ann Heng^{1,2}

¹Department of Computer Science and Engineering, CUHK, Hong Kong, China;

²Institute of Medical Intelligence and XR, CUHK, Hong Kong, China

* Equal contribution, [†] Project lead, Corresponding author
jpli21@cse.cuhk.edu.hk

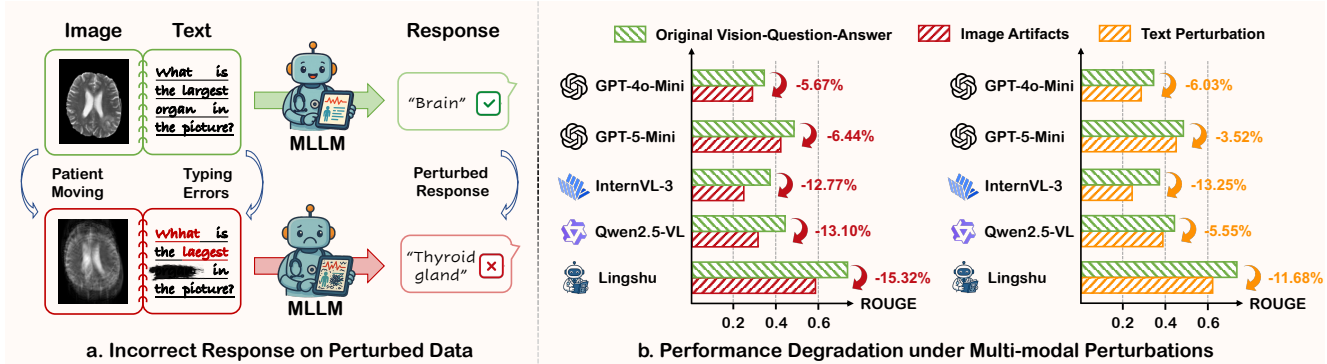


Figure 1. Analysis of MLLM sensitivity to different input perturbations: (a) MLLM produces incorrect responses when inputs contain noise. (b) Comparison between original and perturbed VQA pairs, which demonstrates the performance deterioration of leading MLLMs under visual and textual perturbations (left: CT sparse view artifact, right: character level typographical errors).

Abstract

Medical Multi-modal Large Language Models (MLLMs) have shown promising clinical performance. However, their sensitivity to real-world input perturbations, such as imaging artifacts and textual errors, critically undermines their clinical applicability. Systematic analysis of such noise impact on medical MLLMs remains largely unexplored. Furthermore, while several works have investigated the MLLMs’ robustness in general domains, they primarily focus on text modality and rely on costly fine-tuning. They are inadequate to address the complex noise patterns and fulfill the strict safety standards in medicine. To bridge this gap, this work systematically analyzes the impact of various perturbations on medical MLLMs across both visual and textual modalities. Building on our findings, we introduce a training-free Inherent-enhanced Multi-modal Calibration (IMC) framework that leverages MLLMs’ inherent denoising capabilities following the perceive-and-calibrate principle for cross-modal robustness enhancement. For the visual modality, we propose a Perturbation-aware Denois-

ing Calibration (PDC) which leverages MLLMs’ own vision encoder to identify noise patterns and perform prototype-guided feature calibration. For text denoising, we design a Self-instantiated Multi-agent System (SMS) that exploits the MLLMs’ self-assessment capabilities to refine noisy text through a cooperative hierarchy of agents. We construct a benchmark containing 11 types of noise across both image and text modalities on 2 datasets. Experimental results demonstrate our method achieves the state-of-the-art performance across multiple modalities, showing potential to enhance MLLMs’ robustness in real clinical scenarios.

1. Introduction

Medical Multi-modal Large Language Models (MLLMs) have achieved remarkable progress due to their superior capabilities across various tasks [31, 45, 47] and potential to alleviate clinical workload [51]. However, their robustness in handling input noise remains far from optimal, as minor corruptions in the inputs can lead to dramatic changes in re-

sponses and result in erroneous outputs [42] (as shown in Figure 1(a)). Moreover, compared to the general domain, medical data commonly involve more diverse noise that is difficult to detect, such as equipment deterioration [22], patient motion artifacts [20], or human operational errors [36], leading to significant model performance decrease. Several studies have highlighted the impact of prompt noise on the reliability of LLMs [1, 9, 30, 39]. Existing solutions include layer editing approaches that update targeted parameters [29] and adversarial training methods that expose models to constructed perturbed examples [5]. However, these investigations predominantly focus on text-modality under general domains and require resource-intensive fine-tuning processes, making them unsuitable for clinical practice. In this work, we tackle this critical challenge from two perspectives: 1) Analyzing the impact of prevalent noise types in medical images and questions on medical MLLMs performance; 2) Leveraging these insights to develop a training-free framework for enhancing medical MLLMs robustness.

To systematically quantify the model vulnerability, we propose, to the best of our knowledge, *the first comprehensive benchmark, RobustMed-Bench*, which analyzes the sensitivity of MLLMs to different perturbed inputs under medical scenarios. Our RobustMed-Bench simulates diverse noise across both visual and textual modalities, generating original-noisy data pairs that provide clear insights into model performance variations under distinct noisy conditions. For image modalities, we select six types of image noise commonly arising in three major types of medical imaging, including MRI, CT, and X-ray. For the text modality, we analyze typical patterns in how humans ask medical questions and simulate five prevalent types of noise at both the character level and the sentence level [9]. Extensive experiments on our RobustMed-Bench reveal that existing leading MLLMs show notable performance deterioration under both visual and textual perturbations (as recorded in Figure 1(b)), highlighting the urgent need for robustness improvements to enable safe clinical integration.

To counter this fragility, we propose a training-free Inherent-enhanced Multi-modal Calibration (IMC) framework based on the principle of “perceive-and-calibrate”. Our IMC is built based on the insight that MLLMs can inherently perceive and correct multi-modal noise, whose abilities can be unlocked without any finetuning or external modules. Our experimental results reveal that MLLMs’ vision encoders can effectively extract rich latent information for precise fine-grained classification of different states, distinguishing both normal cases across modalities and specific abnormal patterns up to specific noise types. Based on this finding, we design an effective Perturbation-aware Denoising Calibration (PDC) that utilizes the MLLMs’ built-in vision encoders to compute embedding prototypes and feature gaps between original and noisy images, employing

these results for perturbation classification and fine-grained noise calibration. Meanwhile, we observe that MLLMs demonstrate a capability to partially identify and correct textual errors when properly prompted. Inspired by this, we propose a Self-instantiated Multi-agent System (SMS) for text denoising. The system first parallelly coordinates diverse self-initiated agents for perceiving and removing textual noise. Then it aggregates and refines these denoised outputs with visual information, feeding the result back for the next parallel denoising loop.

Our main contributions are summarized as follows:

- We construct RobustMed-Bench to systematically analyze noise effects on medical MLLMs through a noise simulation pipeline that generates common medical noise types across both image and text modalities.
- We empirically identify that multi-modal perturbations result in substantial performance degradation among existing leading MLLMs through extensive experiments.
- We develop a training-free multi-modal IMC framework consisting of PDC and SMS that both utilize perceive-and-calibrate processes for image and text denoising.
- The experimental results show that our method greatly improves model robustness against diverse noise, advancing the clinical applicability of medical MLLMs.

2. Related Work

2.1. Noise in Medical Multi-Modal Data

Medical data from real-world clinical settings is susceptible to highly complex and diverse types of noise across both image and textual modalities [6, 23, 49]. Medical image noise stems from multiple corruption sources, such as instrumental artifacts [15], environmental factors [40], modality distortions [12], and registration errors [2]. Meanwhile, textual noise in medical data, such as non-standardized language [32] and transcription errors [44], complicates the extraction of accurate semantics. Several recent works have identified the challenge in handling multi-modal noise and tried to tackle it through tailored denoising strategies, such as training additional deep learning-based denoising models [3, 26, 38, 41], employing self-supervised denoising [18, 46, 54], and leveraging data enhancement strategies [21, 25]. However, these studies mainly focus on removing noise in conventional deep learning frameworks. Consequently, a significant gap persists in understanding how multi-modal medical data noise impacts MLLMs, which is vital for the reliability of these advanced models deployed in clinical scenarios. Therefore, in this work, we conduct a systematic investigation and propose solutions for alleviating perturbation impacts on medical MLLMs.

2.2. Sensitivity of LLMs to Perturbations

Prior research has examined the robustness of LLMs to text noise [1, 9, 30, 39], with several studies creating benchmarks for robustness evaluation, such as Lmtry [8], PromptEval [37], and PromptBench [56]. Based on these studies, researchers have attempted to enhance model robustness through additional fine-tuning [43, 50, 53]. However, such computationally expensive approaches are impractical for models that are already deployed. Alternative researches have explored training-free methodologies by employing randomized smoothing [11, 13]. Nevertheless, these methods need extensive noisy samples to achieve reliable smooth distribution and inject random noise to the intermediate states. This data-intensive requirement makes them unsuitable for complex multi-modal data. Although Liu et al. [28] have designed a multi-modal framework for reducing hallucinations in MLLMs, it is not applicable to some types of textual perturbations that introduce out-of-vocabulary tokens beyond the tokenizer’s encoding capacity. Therefore, there is an urgent need to design a comprehensive framework for enhancing model robustness against diverse multi-modal noise types without additional fine-tuning or external models.

3. RobustMed-Bench

To systematically investigate the robustness challenges faced by medical MLLMs in real-world clinical scenarios, we introduce RobustMed-Bench, a comprehensive evaluation benchmark designed to assess model sensitivity to authentic medical data noise. The construction of our benchmark is detailed below, with illustrative noisy cases provided in Figure 2(a).

3.1. Image noise

For image noise construction, we consider three prevalent medical imaging modalities in clinical practice (CT, MRI and X-ray), simulating distinct noise types that are aligned with real clinical scenarios for each modality.

- Noise in CT imaging primarily arises from clinical demands to minimize radiation exposure and enhance scanning efficiency, resulting in *sparse view* [24] and *low dose* [33] noise. Sparse view generates regular stripe artifacts degrading spatial resolution, whereas low dose induces randomly distributed granular noise that impairs contrast resolution. Both types are extremely common in practice.
- MRI noise mainly arises from the longer scanning time required compared to other medical imaging techniques and its inherent hardware constraints. *Patient motion* generates ghosting artifacts that blur anatomical details [10], radio frequency interference creates *banding* noise with regular stripe patterns [7], and insufficient field of view relative to imaged anatomy produces *aliasing* noise with

overlapping structure artifacts [52].

- Unlike other imaging modalities, X-ray acquisition occurs instantaneously, making it highly sensitive to even minimal movements [19]. *Patient movement* or heavy respiratory motion during the scanning process can produce streaking artifacts and reduced contrast resolution.

In RobustMed-Bench, we incorporate different severity levels of these noise into original images from SLAKE [27] and OmniMed [14], due to their rich diversity in medical imaging modalities and question types. In the main paper, we focus on the SLAKE-based dataset, while details of the OmniMed-based dataset are presented in the supplementary. As shown in Figure 2(b), our SLAKE-based benchmark contains 707/343/450 samples for CT/MRI/X-ray modalities respectively, with open-ended and closed-ended questions comprising 64% and 36% of the dataset.

3.2. Text noise

We inject various common typographical errors into question sentences to simulate real-world text input scenarios at both character and sentence levels. For character level noise, we implement four types: 1) random character insertion within words, where arbitrary characters are inserted at random positions to mimic typing mistakes; 2) random character deletion from words, simulating cases where users accidentally miss keystrokes; 3) random character transposition within words, reflecting common finger placement errors where adjacent characters are swapped; 4) random character substitution within words, representing scenarios where users hit incorrect keys due to adjacent key confusion on standard keyboards. For sentence level noise, we recognize that clinicians may provide extraneous information beyond the main question when interacting with MLLMs, such as background context. Therefore, we also incorporate extra sentence noise by adding semantically unrelated sentences alongside the primary medical question.

3.3. Sensitivity of MLLMs to noise

This subsection explores the robustness of multiple state-of-the-art MLLMs against the previously described noise using RobustMed-Bench. We report accuracy and ROUGE-1 scores for closed-ended and open-ended questions respectively, using CT sparse view for visual noise and a random combination of four character noise types for textual disturbances. To maintain clear presentation, complete results for all noise variations are provided in the supplementary material. As shown in Table 1, all tested MLLMs exhibit notable performance degradations under noisy conditions. Closed-source MLLMs (GPT-5-Mini[35] and GPT-4o-Mini[16]) experience approximately 7% and 5% ROUGE score reductions respectively under image noise, and 4% and 6% performance drops under text noise compared to original data. The degradation is more severe for open-source

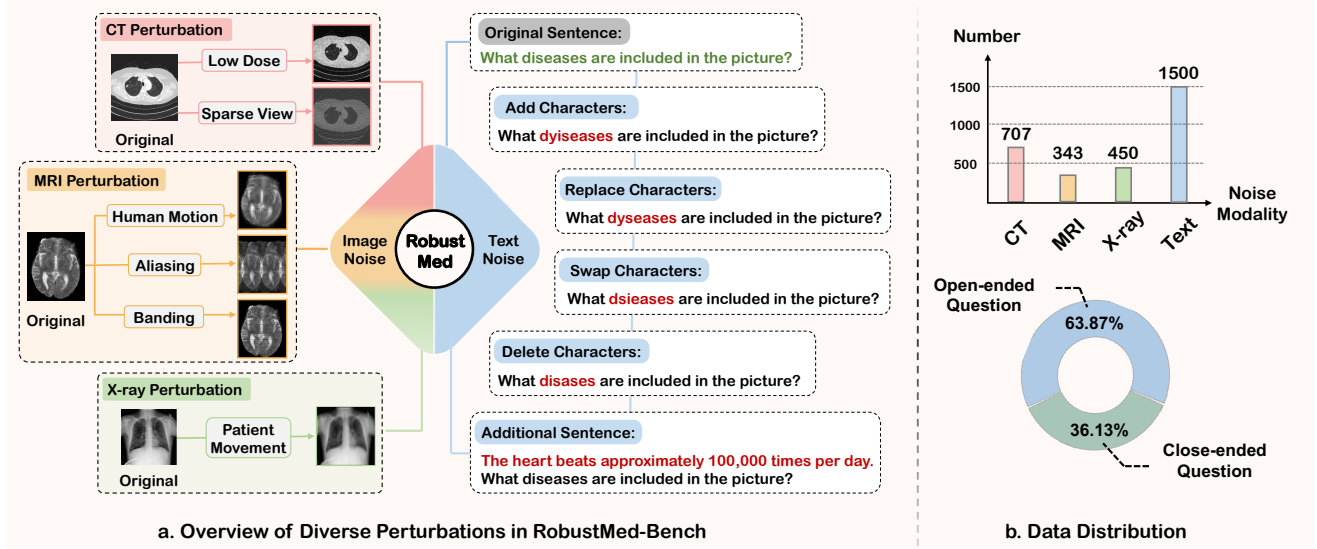


Figure 2. Overview of SLAKE-based RobustMed-Bench dataset composition: (a) Visualization of noise types included in our benchmark. For images, CT contains low dose and sparse view noise, MRI includes human motion, aliasing and banding corruptions, and X-ray with patient movement artifacts. For text, we incorporate four common typographical errors: add/delete/swap/replace characters in words, and additional unrelated sentences noise; (b) Statistical distribution of modalities and question categories of the SLAKE-based benchmark.

Table 1. Performance degradation of MLLMs under CT sparse view artifacts and mixed character level text noise (including randomly delete/add/swap/replace). Subscripts show degradation.

MLLMs	Noise	ACC(\uparrow)	ROUGE(\uparrow)
GPT-5-Mini [35]	Original	79.64	49.23
	CT Sparse View	78.21 $_{-1.43}$	42.78 $_{-6.45}$
	Character Noise	77.14 $_{-2.50}$	45.71 $_{-3.52}$
GPT-4o-Mini [16]	Original	70.71	34.78
	CT Sparse View	65.71 $_{-5.00}$	29.11 $_{-5.67}$
	Character Noise	66.79 $_{-3.92}$	28.75 $_{-6.03}$
InternVL-3-9B [55]	Original	75.71	37.67
	CT Sparse View	64.29 $_{-11.42}$	24.90 $_{-12.77}$
	Character Noise	59.29 $_{-16.42}$	24.42 $_{-13.25}$
Qwen2.5-VL-7B [4]	Original	73.93	44.98
	CT Sparse View	60.71 $_{-13.22}$	31.89 $_{-13.09}$
	Character Noise	66.79 $_{-7.14}$	39.43 $_{-5.55}$
Lingshu-7B [48]	Original	78.57	75.10
	CT Sparse View	77.14 $_{-1.43}$	59.78 $_{-15.32}$
	Character Noise	69.29 $_{-9.28}$	63.42 $_{-11.68}$

MLLMs, including general-domain models (InternVL-3-9B[55], Qwen2.5-VL-7B[4]) and medical-specific model (Lingshu-7B[48]), where performance losses on open-ended questions can reach approximately 13%-15% under image noise. The situation for closed-ended questions is also unsatisfactory. GPT-5-Mini exhibits the highest robustness among all tested MLLMs, showing merely 1.43% and 2.50% accuracy drops under image and text noise, respectively. In contrast, InternVL-3-9B, Qwen2.5-VL-7B suffer more than 10% accuracy loss on image corruption and 16%

and 7% respectively on text noise. Although Lingshu-7B was trained on SLAKE data and shows better robustness on closed-ended questions than other open-source MLLMs, it still struggles with input noise with significant performance drops on open-ended questions. To make a brief summary, current MLLMs demonstrate inadequate robustness against noise in medical datasets, resulting in substantial performance deterioration that presents a major obstacle to practical medical deployment, thus highlighting the urgent need for developing an efficient denoising framework.

4. Method

4.1. Preliminary

In this task, we define several types of noise that can be applied to original Vision(v)-Question(q)-Answer(a) (VQA) pairs $x = (v, q, a)$ by injecting them into either the visual or the textual part of the prompt, resulting in (\tilde{v}, q, a) or (v, \tilde{q}, a) , respectively. Our target is to build a comprehensive framework that enhances MLLM Θ to maintain consistent predictions under perturbations, formally expressed as $\Theta(\tilde{v}, q) \approx \Theta(v, \tilde{q}) \approx \Theta(v, q)$. To improve the robustness of MLLMs while avoiding additional resource costs, we propose a training-free Inherent-enhanced Multi-modal Calibration (IMC) framework focusing on exploring only the model’s inherent capabilities for multi-modal denoising.

4.2. Perturbation-aware Denoising Calibration

We adhere to the “perceive-and-calibrate” principle in designing the image denoising part for visual embedding cal-

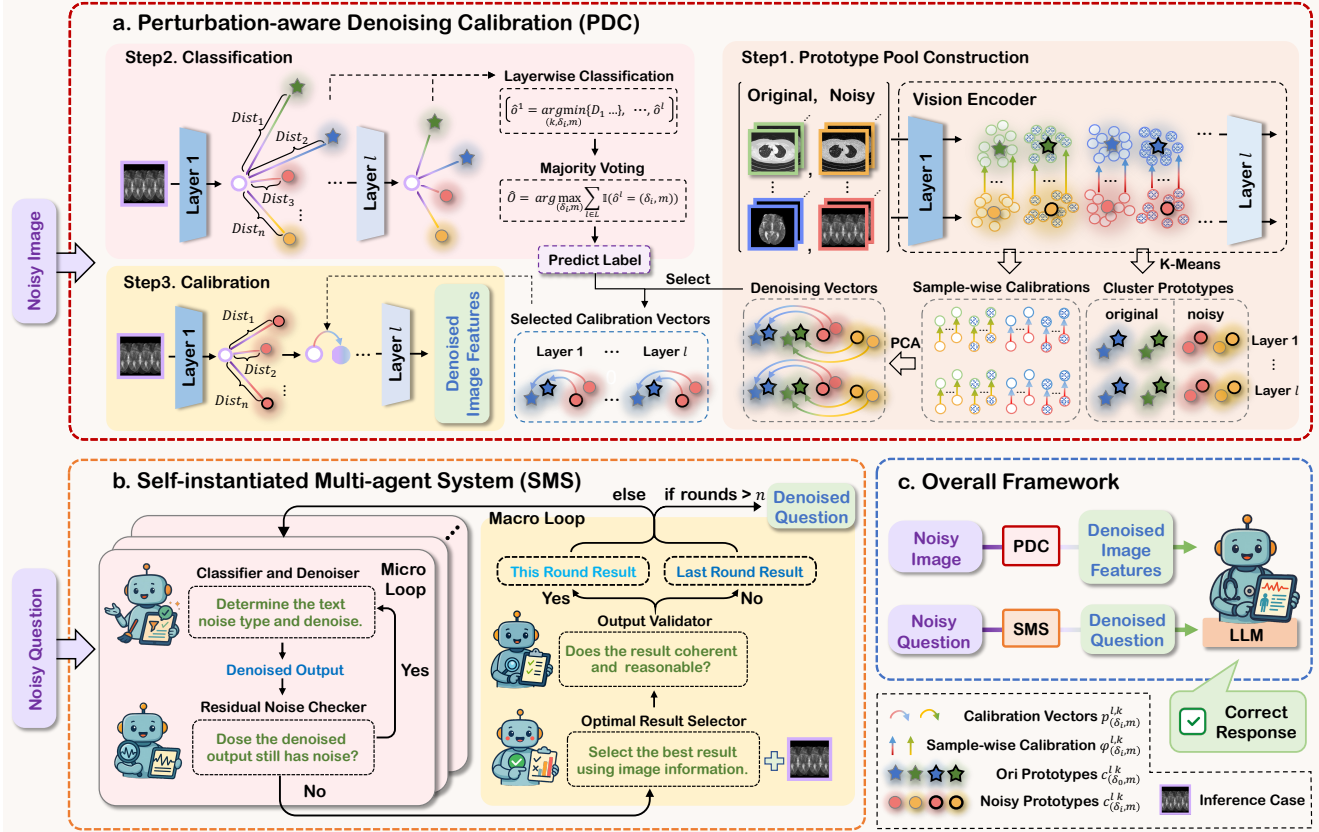


Figure 3. Architecture of our Inherent-enhanced Multi-modal Calibration (IMC) framework, which follows the perceive-and-calibrate process for both image and text modalities. (a) Perturbation-aware Denoising Calibration (PDC) enables image denoising through prototype-guided classification, then applies PCA-based calibration vectors to rectify vision features across all vision encoder layers; (b) Self-instantiated Multi-agent System (SMS) enables text denoising through hierarchical multi-agent coordination with micro and macro iterations that simulate human iterative editing processes; (c) Our framework integrates PDC and SMS for unified multi-modal denoising.

ibration (Figure 3(a)). Specifically, we first perceive the existence and type of noise by recruiting a prototype-based classifier across all vision encoder layers. Afterward, a calibration vector is defined as the direction of principal embeddings from the noisy sample group toward the corresponding normal sample group. Finally, the input noisy embedding is rectified by the calibration vector at each layer. The specific computation process is detailed as follows.

Noise perception. We achieve robust noise classification by constructing a prototype pool. We first extract a group of embeddings $\{f_{(\delta_i, m)}^l\}$ from all samples belonging to modality $m \in M$ and noisy type $\delta_i \in \Delta$ at the l -th layer of the vision encoder. Here, $M = \{\text{CT, MRI, X-ray}\}$ denotes three modalities considered in our experiment, and $\Delta = \{\delta_0, \delta_1, \dots, \delta_n\}$ represents all possible image states, where δ_0 denotes the normal state and $\{\delta_1, \dots, \delta_n\}$ correspond to n types of noise. For each condition (δ_i, m) , we generate a set of K prototypes, $\{c_{(\delta_i, m)}^{l, k}\}_{k=1}^K$, by applying K-Means [17] clustering to the corresponding embeddings:

$$\{c_{(\delta_i, m)}^{l, k}\}_{k=1}^K = \text{KMeans}(\{f_{(\delta_i, m)}^l\}), \quad (1)$$

where each prototype $c_{(\delta_i, m)}^{l, k}$ represents the cluster center of embeddings obtained from state (δ_i, m) and feature layer l . During the inference stage, the image of the incoming sample \hat{v} is fed into the vision encoder to obtain the layerwise embeddings $\{\hat{f}^l\}_{l=1}^L$. For each layer, we select the nearest prototype $\hat{c}_{(\delta_i, m)}^{l, k}$ for \hat{f}^l from all prototypes at the same layer, denoted as $\{\hat{c}_{(\delta_i, m)}^{l, k}\}_{k, \delta_i, m \in K \times \Delta \times M}$. Thus, we obtain the classified result $\hat{o}^l = (\hat{\delta}_i^l, \hat{m}^l)$ at the l -th layer, including noise type and modality based on the identification of $\hat{c}_{(\delta_i, m)}^{l, k}$ by calculating the feature distance $\text{Dist}(\cdot, \cdot)$:

$$\hat{o}^l = (\hat{\delta}_i^l, \hat{m}^l) = \arg \min_{k, \delta_i, m \in K \times \Delta \times M} \text{Dist}(\hat{f}^l, \hat{c}_{(\delta_i, m)}^{l, k}). \quad (2)$$

Finally, we aggregate the predictions from all layers and apply majority voting to classify the image as the type that

appears most frequently across layers:

$$\hat{o}_v = \arg \max_{(\delta_i, m)} \sum_{l \in L} \mathbb{I}(\hat{o}^l = (\delta_i, m)), \quad (3)$$

where $\mathbb{I}(\cdot)$ is the indicator function that returns 1 if the condition is true and 0 otherwise. The final classification result is denoted as $\hat{o}_v = (\hat{\delta}_i, \hat{m})$. If the predicted $\hat{\delta}_i = \delta_0$, we determine this is a normal image and process it directly. Otherwise, the image is forwarded to the calibration pipeline.

Embedding calibration. After determining the noise type $\hat{\delta}_i$ and modality \hat{m} , we perform finer-grained selection at each layer to mitigate potential layer-wise misclassifications before majority voting. We select the optimal cluster \hat{k} at each layer that is closest to the incoming embedding under the state $(\hat{\delta}_i, \hat{m})$ similar to Eq. 2. Subsequently, the sample-wise calibration directions $\varphi_{(\hat{\delta}_i, \hat{m}), j}^{l, \hat{k}}$ are computed by subtracting the embeddings of noisy samples from the corresponding embeddings of normal samples:

$$\varphi_{(\hat{\delta}_i, \hat{m}), j}^{l, \hat{k}} = f_{(\hat{\delta}_0, \hat{m}), j}^{l, \hat{k}} - f_{(\hat{\delta}_i, \hat{m}), j}^{l, \hat{k}}, \quad \delta_i \neq \delta_0. \quad (4)$$

where $j \in \mathcal{G}_{(\hat{\delta}_i, \hat{m})}^{l, \hat{k}}$ which denotes the set of sample indices associated with the \hat{k} -th cluster under the $(\hat{\delta}_i, \hat{m})$ state at the l -th layer. Afterward, we derive the final calibration vector for the calibration direction group using the PCA algorithm:

$$p_{(\hat{\delta}_i, \hat{m})}^{l, \hat{k}} = \text{PCA}(\{\varphi_{(\hat{\delta}_i, \hat{m}), j}^{l, \hat{k}}\}), \quad j \in \mathcal{G}_{(\hat{\delta}_i, \hat{m})}^{l, \hat{k}}. \quad (5)$$

This calibration vector can be interpreted as a perturbation-specific transformation in the latent space, guiding noisy embeddings toward the correct feature space. During the embedding calibration process, the selected layer-wise calibration vectors are applied to rectify the embeddings of the noisy image at each vision encoder layer, with a calibration weight α controlling the modification severity: $\hat{f}^l = \hat{f}^l + \alpha \cdot p_{(\hat{\delta}_i, \hat{m})}^{l, \hat{k}}$. The final denoised visual embedding will be served as the input for downstream LLM reasoning:

$$\text{Response} = LLM(\hat{f}^L, \hat{q}). \quad (6)$$

4.3. Self-instantiated Multi-agent System

The text denoising module employs a self-instantiated multi-agent system consisting of two loops (Figure 3(b)). Specifically, the micro loop first perceives and removes textual noise. The macro loop then selects and refines outputs from multiple parallel micro loop iterations, feeding the refined result back as input for subsequent micro loops.

Micro loop incorporates an agent called the *Classifier and Denoiser* which receives input sentences to identify noise types and performs corresponding noise removal operations. Subsequently, another agent called the *Residual Noise Checker* determines whether the denoised results

from previous step still contain noise, and if noise is detected, it invokes the *Denoiser* again to perform additional denoising operations. The micro loop terminates only when the *Residual Noise Checker* confirms that the current result contains no more perturbations. We perform this process k times in parallel, yielding k responses from the micro loops to broaden the range of denoising outcomes and thereby increase the probability of obtaining correct results.

Macro loop deploys a new agent named *Optimal Result Selector*, which integrates the k denoised results from the micro loop together with the input image and selects the result that is both noise-free and consistent with the image content. To ensure the quality of the macro loop output, we introduce an *Output Validator* that evaluates whether the result from previous *Optimal Result Selector* represents a coherent and logically consistent sentence, thus mitigating potential confusion that may manifest in some MLLMs with limited language reasoning capabilities. If the output is valid, we forward the updated sentence to the *Denoiser* for the next micro loop iteration with a halved temperature parameter to enable finer-grained adjustments; otherwise, we forward the original input sentence from the current round to prevent the propagation of additional noise. This hierarchical process ends when the macro loop reaches its predefined maximum number of rounds n , and the final denoised sentence is served as the new prompt for MLLM inference.

5. Experiment

5.1. Implementation Details

We construct two perturbed datasets with VQA pairs derived from SLAKE [27] and OmniMed [14], and we present the experimental results on SLAKE-based dataset in the main paper, while results on the OmniMed-based dataset are provided in the supplementary material. We use Qwen2.5-VL-7B [4] as our base model for all experiments in this section. In this paper, the number of selected sample pairs for building the prototype pool is 100 and the number of clusters is 8. The number of parallel micro loops k is set to 10 and the number of macro loop rounds n is set to 2. The calibration weight α is set to 0.05. All experiments were carried out on 2 NVIDIA RTX A6000 GPUs (48 GB). We evaluate model performance using Accuracy on closed-ended questions and ROUGE-1, BLEU, and Recall on open-ended questions. We compare our IMC method with state-of-the-art methods: 1) Robustness of Prompting (RoP) [34] employs few-shot prompting to enhance robustness; 2) Self-Denoising (SD) [1] adopts prompt engineering; and 3) Visual and Textual Intervention (VTI) [28] utilizes embedding rectifications for hallucination reduction.

Table 2. Performance comparison of MLLM robustness across six medical imaging artifacts, subscripts denote performance drops. **Bold** font denotes the best performance.

Method	ACC(↑)	ROUGE(↑)	BLEU(↑)	Recall(↑)
MRI Original VQA				
Base Model	77.05	45.95	8.07	45.23
MRI Human Motion				
Base Model	70.49 _{-6.56}	39.51 _{-6.44}	7.10 _{-0.97}	39.56 _{-5.67}
RoP [34]	59.02 _{-18.03}	37.94 _{-8.01}	6.89 _{-1.18}	39.60 _{-5.63}
SD [1]	73.77 _{-3.28}	36.46 _{-9.49}	6.45 _{-1.62}	38.27 _{-6.96}
VTI [28]	73.77 _{-3.28}	40.17 _{-5.78}	7.01 _{-1.06}	39.45 _{-5.78}
Ours	75.41 _{-1.64}	42.27 _{-3.68}	7.49 _{-0.58}	41.36 _{-3.87}
MRI Aliasing				
Base Model	54.10 _{-22.95}	18.36 _{-27.59}	3.22 _{-4.85}	17.92 _{-27.31}
RoP [34]	54.10 _{-22.95}	31.12 _{-14.83}	5.61 _{-2.46}	31.38 _{-13.85}
SD [1]	55.74 _{-21.31}	28.01 _{-17.94}	4.98 _{-3.09}	28.94 _{-16.29}
VTI [28]	55.74 _{-21.31}	20.88 _{-25.07}	3.47 _{-4.60}	19.01 _{-26.22}
Ours	60.26 _{-16.79}	31.64 _{-14.31}	5.65 _{-2.42}	31.61 _{-13.62}
MRI Banding				
Base Model	75.41 _{-1.64}	43.86 _{-2.09}	7.65 _{-0.42}	42.51 _{-2.72}
RoP [34]	70.49 _{-6.56}	41.21 _{-4.74}	7.23 _{-0.84}	40.67 _{-4.56}
SD [1]	73.77 _{-3.28}	41.27 _{-4.68}	7.07 _{-1.00}	41.33 _{-3.90}
VTI [28]	76.29 _{-0.76}	44.15 _{-1.80}	7.71 _{-0.36}	43.58 _{-1.65}
Ours	77.00 _{-0.05}	45.52 _{-0.43}	7.94 _{-0.13}	45.16 _{-0.07}
CT Original VQA				
Base Model	73.48	46.07	8.18	45.88
CT Sparse View				
Base Model	59.85 _{-13.63}	33.70 _{-12.37}	6.01 _{-2.17}	33.17 _{-12.71}
RoP [34]	63.64 _{-9.84}	31.61 _{-14.46}	5.63 _{-2.55}	31.32 _{-14.56}
SD [1]	62.12 _{-11.36}	30.64 _{-15.43}	5.66 _{-2.52}	35.69 _{-10.19}
VTI [28]	56.06 _{-17.42}	32.41 _{-13.66}	5.87 _{-2.31}	32.93 _{-12.95}
Ours	63.14 _{-10.34}	36.59 _{-9.48}	6.47 _{-1.71}	36.73 _{-9.15}
CT Low Dose				
Base Model	65.91 _{-7.57}	36.53 _{-9.54}	6.55 _{-1.63}	36.91 _{-8.97}
RoP [34]	65.91 _{-7.57}	35.30 _{-10.77}	6.01 _{-2.17}	34.25 _{-11.63}
SD [1]	69.70 _{-3.78}	40.14 _{-5.93}	7.06 _{-1.12}	42.16 _{-3.72}
VTI [28]	61.36 _{-12.12}	34.29 _{-11.78}	6.12 _{-2.06}	34.88 _{-11.00}
Ours	67.92 _{-5.56}	41.10 _{-4.97}	7.31 _{-0.87}	39.61 _{-6.27}
X-ray Original VQA				
Base Model	88.89	53.68	7.54	40.41
X-ray Patient Movement				
Base Model	80.56 _{-8.33}	47.83 _{-5.85}	6.40 _{-1.14}	34.59 _{-5.82}
RoP [34]	63.89 _{-25.00}	42.23 _{-11.45}	5.53 _{-2.01}	32.07 _{-8.34}
SD [1]	73.61 _{-15.28}	45.66 _{-8.02}	6.37 _{-1.17}	35.73 _{-4.68}
VTI [28]	79.17 _{-9.72}	50.77 _{-2.91}	7.10 _{-0.44}	38.89 _{-1.52}
Ours	87.50 _{-1.39}	51.99 _{-1.69}	7.24 _{-0.30}	39.67 _{-0.74}

5.2. Performance on Image Noise

Table 2 shows that the MLLM suffers performance drop under six image noise types across three medical modalities, confirming insufficient robustness against image perturbations. Specifically, on open-ended questions, the base model accuracy drops by 6.56%, 22.95%, and 1.64% for MRI (human motion, aliasing, banding), 13.63% and 7.57%

for CT (sparse view, low dose), and 8.33% for X-ray patient movement. Meanwhile, on closed-ended questions, the ROUGE scores degrade across all noise types, with drops ranging from 2.09% (MRI banding) to 27.59% (MRI aliasing). Notably, the base MLLM suffers particularly severe deterioration on MRI aliasing, as aliasing creates overlapping artifacts that destroy the overall image structure, unlike other noise types that only affect details and resolution.

Comparison Methods. The comparison methods RoP and SD exhibit improvements only in specific scenarios (12.67%/9.65% higher ROUGE scores under MRI aliasing and 3.79%/2.27% ACC increases under CT sparse view), indicating their substantial limitations and poor generalizability to diverse noise types. Similarly, VTI shows unstable performance, achieving 4.3% higher recall on X-ray patient movement but deteriorating on CT noise types, even performing worse than the original model. This occurs because it employs only a single direction calibration, which is inadequate for diverse scenarios and may adversely pull the vision features further away from the correct feature space.

Our Approach. Compared to other methods, our proposed IMC framework is more robust and stable, bringing consistent performance improvement across all noise types. Notably, our algorithm attains a substantial 13.28% ROUGE score enhancement on open-ended questions under MRI aliasing and achieves 6.94% accuracy improvement on closed-ended questions under X-ray patient movement. This experiment indicates that our IMC framework can effectively enhance the robustness of MLLMs against various image artifacts, laying a solid foundation for the reliability of medical MLLMs in practical clinical applications.

5.3. Performance on Text Noise

Similar to vision artifacts, Table 3 demonstrates the sensitivity of the base MLLM to five noise types, resulting in clear performance drops. Specifically, the model exhibits consistent sensitivity patterns across diverse character perturbations, with closed-ended question accuracy declining by 1.84% to 5.35% and open-ended question metrics showing average reductions of approximately 4.5% for ROUGE and 3% for BLEU. The MLLM shows more severe accuracy deterioration under unrelated sentence noise, experiencing a 19.97% performance decline on closed-ended questions and 10.03% ROUGE drops on open-ended questions. Moreover, the degradation variance from these character-level modifications is smaller than from vision noise, likely due to the comparable perturbation severity that fall beyond the textual tokenizer’s effective encoding range.

Comparison Methods. The comparison methods RoP and SD cannot effectively reduce textual noise influence, as they lack the ability to identify textual corruptions and the noise contaminates the entire processing context. Meanwhile, VTI performs more inconsistently on text noise com-

pared to vision corruptions, yielding several negative effects across all noise types. This may result from the inadequacy of latent space steering in calibrating perturbations, particularly when noisy words (e.g., “these” becoming “th” and “ese”) induce out-of-vocabulary tokens for the tokenizer.

Our Approach. Conversely, our approach demonstrates effective robustness improvement by creating iterative multi-agent system. Specifically, under random character deletion noise, we achieve 2.41% ROUGE improvement on open-ended questions and 2.67% accuracy increase on closed-ended questions. The improvements become even more pronounced under unrelated sentences perturbation, reaching 5.03% and 12.73% respectively. This experiment strongly supports that our IMC framework can effectively reduce MLLMs’ sensitivity to different textual noise types.

Table 3. Performance comparison of MLLM robustness across five text perturbation types, subscripts denote performance drops. **Bold** font denotes the best performance.

Method	ACC(↑)	ROUGE(↑)	BLEU(↑)	Recall(↑)
Original VQA				
Base Model	75.09	49.71	7.93	44.96
Delete Characters				
Base Model	70.58 _{-4.51}	44.17 _{-5.54}	7.08 _{-0.85}	40.70 _{-4.26}
RoP [34]	68.82 _{-6.27}	37.04 _{-12.67}	5.91 _{-2.02}	36.39 _{-8.57}
SD [1]	73.06 _{-2.03}	39.38 _{-10.33}	6.18 _{-1.75}	37.53 _{-7.43}
VTI [28]	70.10 _{-4.99}	42.16 _{-7.55}	6.84 _{-1.09}	39.17 _{-5.79}
Ours	73.25 _{-1.84}	46.58 _{-3.13}	7.45 _{-0.48}	42.39 _{-2.57}
Add Characters				
Base Model	73.25 _{-1.84}	45.32 _{-4.39}	7.34 _{-0.59}	42.19 _{-2.77}
RoP [34]	73.80 _{-1.29}	38.94 _{-10.77}	5.97 _{-1.96}	38.21 _{-6.75}
SD [1]	72.51 _{-2.58}	38.38 _{-11.33}	6.01 _{-1.92}	37.32 _{-7.64}
VTI [28]	72.76 _{-2.33}	45.59 _{-4.12}	7.21 _{-0.72}	41.44 _{-3.52}
Ours	73.43 _{-1.66}	47.45 _{-2.26}	7.77 _{-0.16}	43.41 _{-1.55}
Swap Characters				
Base Model	69.74 _{-5.35}	44.42 _{-5.29}	7.19 _{-0.74}	41.26 _{-3.70}
RoP [34]	62.55 _{-12.54}	35.32 _{-14.39}	5.44 _{-2.49}	33.63 _{-11.33}
SD [1]	68.27 _{-6.82}	37.73 _{-11.98}	5.91 _{-2.02}	36.40 _{-8.56}
VTI [28]	67.81 _{-7.28}	43.88 _{-5.83}	7.11 _{-0.82}	40.69 _{-4.27}
Ours	69.93 _{-5.16}	45.30 _{-4.41}	7.32 _{-0.61}	41.03 _{-3.93}
Replace Characters				
Base Model	70.48 _{-4.61}	45.03 _{-4.68}	7.18 _{-0.75}	41.23 _{-3.73}
RoP [34]	65.87 _{-9.22}	35.20 _{-14.51}	5.46 _{-2.47}	34.64 _{-10.32}
SD [1]	70.11 _{-4.98}	38.45 _{-11.26}	5.94 _{-1.99}	36.99 _{-7.97}
VTI [28]	70.86 _{-4.23}	43.81 _{-5.90}	7.16 _{-0.77}	40.47 _{-4.49}
Ours	71.59 _{-3.50}	46.96 _{-2.75}	7.62 _{-0.31}	42.64 _{-2.32}
Unrelated Sentences				
Base Model	58.12 _{-16.97}	39.68 _{-10.03}	6.38 _{-1.55}	37.00 _{-7.96}
RoP [34]	54.23 _{-20.86}	32.74 _{-16.97}	5.56 _{-2.37}	34.83 _{-10.13}
SD [1]	64.22 _{-10.87}	36.84 _{-12.87}	6.38 _{-1.55}	38.86 _{-6.10}
VTI [28]	67.62 _{-7.47}	41.73 _{-7.98}	6.81 _{-1.12}	38.14 _{-6.82}
Ours	70.85 _{-4.24}	44.71 _{-4.99}	7.17 _{-0.76}	40.77 _{-4.19}

5.4. Ablation Study

To further validate our approach, we investigate the impact of layer-wise prototype numbers for image denoising and the number of macro loop iterations for textual processing.

5.4.1. Prototype Numbers for Image Denoising

We hypothesize that a larger number of prototypes yields finer-grained calibration direction vectors, thereby enhancing the precision of noisy embedding rectification. This ablation study explores the impact of varying prototype numbers (1, 2, 4, 8, and 16) on denoising effectiveness under CT low dose setting with 100 sample pairs for building prototype pool. As shown in Table 4, ROUGE scores on open-ended questions gradually improve as the number of clusters increases, reaching the highest score of 41.10% at 8 prototypes, while further increasing to 16 prototypes leads to performance degradation. This phenomenon arises from the fact that finer-grained feature distribution partitioning provides more precise noise removal. However, given the constraint of limited sample pairs, excessive division could introduce additional biases, resulting in performance drop.

Table 4. Ablation on prototype numbers under CT low dose noise.

Clusters	ACC(↑)	ROUGE(↑)	BLEU(↑)	Recall(↑)
1	61.36	34.29	6.12	34.88
2	65.15	36.59	6.63	37.53
4	62.88	37.38	6.48	37.80
8	67.92	41.10	7.31	39.61
16	69.70	37.80	6.82	37.42

5.4.2. Macro Loop Rounds for Textual Denoising

For textual noise processing in our IMC framework, the number of macro loop rounds can directly control the final denoising quality, but it also increases the time complexity. To optimize this trade-off, we explore the relationship between macro loop rounds and denoising quality, evaluating configurations with 1 to 4 loop iterations. We perform experiments using character level random swap noise to facilitate fair comparison. As demonstrated in Table 5, while ROUGE, BLEU, and Recall scores on open-ended questions increase with loop rounds, but the marginal improvements become negligible after 2 rounds. In order to balance the time complexity with performance, and considering the minimal improvement on close-ended questions, we set the loop rounds to 2 in our implementation.

6. Conclusion

In this paper, we introduce the RobustMed-Bench that is designed to simulate various noise types in medical multi-modal data. Our experimental analysis shows that MLLMs exhibit significant performance degradation across different

Table 5. Macro loop rounds ablation under character swap noise.

Loop Rounds	ACC(\uparrow)	ROUGE(\uparrow)	BLEU(\uparrow)	Recall(\uparrow)
1	68.27	41.86	6.79	38.28
2	69.93	45.30	7.32	41.03
3	69.56	45.32	7.32	41.43
4	68.63	46.05	7.48	42.19

modalities when exposed to input perturbations. To address this issue, we develop a training-free framework called Inherent-enhanced Multi-modal Calibration (IMC) consisting of Perturbation-aware Denoising Calibration (PDC) and Self-instantiated Multi-agent System (SMS), which leverages MLLMs' inherent capability through a perceive-and-calibrate paradigm for multi-modal noise removal. This study represents the pioneering effort in benchmarking and enhancing the robustness of medical MLLMs, significantly improving their practical clinical applicability.

References

[1] Aryan Agrawal, Lisa Alazraki, Shahin Honarvar, and Marek Rei. Enhancing llm robustness to perturbed instructions: An empirical study. *arXiv preprint arXiv:2504.02733*, 2025. 2, 3, 6, 7, 8

[2] Goram Mufarrah Alshmrani, Qiang Ni, Richard Jiang, and Nada Muhammed. Hyper-dense_lung_seg: Multimodal-fusion-based modified u-net for lung tumour segmentation using multimodality of ct-pet scans. *Diagnostics*, 13(22):3481, 2023. 2

[3] Dinesh Kumar Atal. Optimal deep cnn-based vectorial variation filter for medical image denoising. *Journal of Digital Imaging*, 36(3):1216–1236, 2023. 2

[4] Shuai Bai, Keqin Chen, Xuejing Liu, Jialin Wang, Wenbin Ge, Sibo Song, Kai Dang, Peng Wang, Shijie Wang, Jun Tang, et al. Qwen2. 5-vl technical report. *arXiv preprint arXiv:2502.13923*, 2025. 4, 6

[5] Shengyuan Bai, Qibin Li, Zhe Wang, Nai Zhou, and Nianmin Yao. Enhancing nlu in large language models using adversarial noisy instruction tuning. In *Proceedings of the AAAI Conference on Artificial Intelligence*, pages 23451–23459, 2025. 2

[6] Zhenyu Cheng, Boyuan Zhang, Yanbo Hu, Yue Du, Tianyong Liu, Zhenxi Zhang, Chang Lu, Shoujun Zhou, and Zhuoxu Cui. Med-diffusion: Diffusion model-based imputation of multimodal sensor data for surgical patients. *Sensors*, 2025. 2

[7] Aaron Defazio, Tullie Murrell, and Michael Recht. Mri banding removal via adversarial training. *Advances in Neural Information Processing Systems*, 33:7660–7670, 2020. 3

[8] Avia Efrat, Or Honovich, and Omer Levy. Lmentry: A language model benchmark of elementary language tasks. In *Findings of the Association for Computational Linguistics: ACL 2023*, pages 10476–10501, 2023. 3

[9] Jiasheng Gu, Hongyu Zhao, Hanzi Xu, Liangyu Nie, Hongyuan Mei, and Wenpeng Yin. Robustness of learning from task instructions. In *Findings of the association for computational linguistics: ACL 2023*, pages 13935–13948, 2023. 2, 3

[10] Inger Havsteen, Anders Ohlhues, Kristoffer H Madsen, Janus Damm Nybing, Hanne Christensen, and Anders Christensen. Are movement artifacts in magnetic resonance imaging a real problem?—a narrative review. *Frontiers in neurology*, 8:232, 2017. 3

[11] Bowei He, Lihao Yin, Hui-Ling Zhen, Jianping Zhang, Lanqing Hong, Mingxuan Yuan, and Chen Ma. Certifying language model robustness with fuzzed randomized smoothing: An efficient defense against backdoor attacks. *arXiv preprint arXiv:2502.06892*, 2025. 3

[12] K Hemalatha, PR Vishnu Vardhan, Alfred Dharmaraj Aravindraj, and S Hari Hara Sudhan. Masked and noise-masked multimodal brain tumor image segmentation using segformer and shared encoder framework. *IEEE Access*, 2025. 2

[13] Jinwei Hu, Yi Dong, Zhengtao Ding, and Xiaowei Huang. Enhancing robustness of llm-driven multi-agent systems through randomized smoothing. *arXiv preprint arXiv:2507.04105*, 2025. 3

[14] Yutao Hu, Tianbin Li, Quanfeng Lu, Wenqi Shao, Junjun He, Yu Qiao, and Ping Luo. Omnimedvqa: A new large-scale comprehensive evaluation benchmark for medical lvlm. In *Proceedings of the IEEE/CVF Conference on Computer Vision and Pattern Recognition*, pages 22170–22183, 2024. 3, 6, 12

[15] Ling Huang, Su Ruan, Pierre Decazes, and Thierry Deneœux. Deep evidential fusion with uncertainty quantification and reliability learning for multimodal medical image segmentation. *Information Fusion*, 113:102648, 2025. 2

[16] Aaron Hurst, Adam Lerer, Adam P Goucher, Adam Perelman, Aditya Ramesh, Aidan Clark, AJ Ostrow, Akila Welihinda, Alan Hayes, Alec Radford, et al. Gpt-4o system card. *arXiv preprint arXiv:2410.21276*, 2024. 3, 4, 12, 13

[17] Anil K Jain and Richard C Dubes. *Algorithms for clustering data*. Prentice-Hall, Inc., 1988. 5

[18] Sun-Young Jeon, Sen Wang, Adam S Wang, Garry E Gold, and Jang-Hwan Choi. Unsupervised training of a dynamic context-aware deep denoising framework for low-dose fluoroscopic imaging. *IEEE Transactions on Instrumentation and Measurement*, 2025. 2

[19] Karim S Karim and Steven Tilley II. Portable single-exposure dual-energy x-ray detector for improved point-of-care diagnostic imaging. *Military Medicine*, 188(Supplement_6):84–91, 2023. 3

[20] G Kavitha, Chetana Prakash, Majid Alhomrani, N Pradeep, Abdulhakeem S Alamri, Piyush Kumar Pareek, and Musah Alhassan. Noise estimation and type identification in natural scene and medical images using deep learning approaches. *Contrast Media & Molecular Imaging*, 2023(1):3923667, 2023. 2

[21] Aghiles Kebaili, Jérôme Lapuyade-Lahorgue, and Su Ruan. Deep learning approaches for data augmentation in medical imaging: a review. *Journal of imaging*, 9(4):81, 2023. 2

[22] MC Kelvin-Agwu, Mojeed Omotayo Adelodun, Geneva Tamunobaraifiri Igwama, and Evangel Chinyere

Anyanwu. The impact of regular maintenance on the longevity and performance of radiology equipment. *Unpublished*, 2024. 2

[23] Sachin Kumar, Sita Rani, Shivani Sharma, and Hong Min. Multimodality fusion aspects of medical diagnosis: A comprehensive review. *Bioengineering*, 11(12):1233, 2024. 2

[24] Hoyeon Lee, Jongha Lee, Hyeongseok Kim, Byungchul Cho, and Seungryong Cho. Deep-neural-network-based sinogram synthesis for sparse-view ct image reconstruction. *IEEE Transactions on Radiation and Plasma Medical Sciences*, 3(2):109–119, 2018. 3

[25] Luc Lerch, Lukas S Huber, Amith Kamath, Alexander Pöllinger, Aurélie Pahud de Mortanges, Verena C Obmann, Florian Dammann, Walter Senn, and Mauricio Reyes. Dreamon: a data augmentation strategy to narrow the robustness gap between expert radiologists and deep learning classifiers. *Frontiers in Radiology*, 4:1420545, 2024. 2

[26] Yuqin Li, Ke Zhang, Weili Shi, Yu Miao, and Zhengang Jiang. A novel medical image denoising method based on conditional generative adversarial network. *Computational and Mathematical Methods in Medicine*, 2021(1):9974017, 2021. 2

[27] Bo Liu, Li-Ming Zhan, Li Xu, Lin Ma, Yan Yang, and Xiao-Ming Wu. Slake: A semantically-labeled knowledge-enhanced dataset for medical visual question answering. In *2021 IEEE 18th international symposium on biomedical imaging (ISBI)*, pages 1650–1654. IEEE, 2021. 3, 6

[28] Sheng Liu, Haotian Ye, Lei Xing, and James Zou. Reducing hallucinations in vision-language models via latent space steering. *arXiv preprint arXiv:2410.15778*, 2024. 3, 6, 7, 8

[29] Shuhan Liu, Xing Hu, Kerui Huang, Xiaohu Yang, David Lo, and Xin Xia. Improving code llm robustness to prompt perturbations via layer-aware model editing. *arXiv preprint arXiv:2507.16407*, 2025. 2

[30] Zhenyi Lu, Jie Tian, Wei Wei, Xiaoye Qu, Yu Cheng, Wenfeng Xie, and Dangyang Chen. Mitigating boundary ambiguity and inherent bias for text classification in the era of large language models. In *Findings of the Association for Computational Linguistics: ACL 2024*, pages 7841–7864, 2024. 2, 3

[31] Siqi Ma, Jiajie Huang, Bolin Yang, Fan Zhang, Jinlin Wu, Yue Shen, Guohui Fan, Zhu Zhang, and Zelin Zang. Medla: A logic-driven multi-agent framework for complex medical reasoning with large language models. *arXiv preprint arXiv:2509.23725*, 2025. 1

[32] Corentin Meyer, Norma Beatriz Romero, Teresinha Evangelista, Brunot Cadot, Jocelyn Laporte, Anne Jeannin-Girardon, Pierre Collet, Ali Ayadi, Kirsley Chennen, and Olivier Poch. Impatient: An integrated web application to digitize, process and explore multimodal patient data. *Journal of Neuromuscular Diseases*, 11(4):855–870, 2024. 2

[33] Taylor R Moen, Baiyu Chen, David R Holmes III, Xinhui Duan, Zhicong Yu, Lifeng Yu, Shuai Leng, Joel G Fletcher, and Cynthia H McCollough. Low-dose ct image and projection dataset. *Medical physics*, 48(2):902–911, 2021. 3

[34] Lin Mu, Guowei Chu, Li Ni, Lei Sang, Zhize Wu, Peiquan Jin, and Yiwen Zhang. Robustness of prompting: Enhancing robustness of large language models against prompting attacks. *arXiv preprint arXiv:2506.03627*, 2025. 6, 7, 8

[35] OpenAI. Introducing gpt-5, 2025. 3, 4, 12, 13

[36] Nana Owusu and Vincent A Magnotta. Factors influencing daily quality assurance measurements of magnetic resonance imaging scanners. *Radiological Physics and Technology*, 14(4):396–401, 2021. 2

[37] Felipe Maia Polo, Ronald Xu, Lucas Weber, Mírian Silva, Onkar Bhardwaj, Leshem Choshen, Allysson Flavio Melo de Oliveira, Yuekai Sun, and Mikhail Yurochkin. Efficient multi-prompt evaluation of llms. *arXiv preprint arXiv:2405.17202*, 2024. 3

[38] Md Ashequr Rahman, Zitong Yu, Barry A Siegel, and Abhinav K Jha. A task-specific deep-learning-based denoising approach for myocardial perfusion spect. In *Proceedings of SPIE—the International Society for Optical Engineering*, page 1246719, 2023. 2

[39] Amirhossein Razavi, Mina Soltangheis, Negar Arabzadeh, Sara Salamat, Morteza Zihayat, and Ebrahim Bagheri. Benchmarking prompt sensitivity in large language models. In *European Conference on Information Retrieval*, pages 303–313. Springer, 2025. 2, 3

[40] Shehanaz Shaik and Sitaramanjaneya Reddy Guntur. Classification of artifacts in multimodal fused images using transfer learning with convolutional neural networks. *Current Medical Imaging*, 20(1):e15734056256872, 2024. 2

[41] Aakansha Soy and Vasani Vaibhav Prakash. Medical image denoising using deep convolutional autoencoders for ultrasound. In *2025 International Conference on Automation and Computation (AUTOCOM)*, pages 262–267. IEEE, 2025. 2

[42] Francesco Villani, Igor Maljkovic, Dario Lazzaro, Angelo Sotgiu, Antonio Emanuele Cinà, and Fabio Roli. Robust image classification with multi-modal large language models. *Pattern Recognition Letters*, 2025. 2

[43] Xiaohua Wang, Zisu Huang, Feiran Zhang, Zhibo Xu, Cenyuan Zhang, Qi Qian, Xiaoqing Zheng, and Xuanjing Huang. Enhancing the capability and robustness of large language models through reinforcement learning-driven query refinement. *arXiv preprint arXiv:2407.01461*, 2024. 3

[44] Keshara Weersasinghe, Saahith Janapati, Xueren Ge, Sion Kim, Sneha Iyer, John A Stankovic, and Homa Alemzadeh. Real-time multimodal cognitive assistant for emergency medical services. *arXiv preprint arXiv:2403.06734*, 2024. 2

[45] Hanguang Xiao, Feizhong Zhou, Xingyue Liu, Tianqi Liu, Zhipeng Li, Xin Liu, and Xiaoxuan Huang. A comprehensive survey of large language models and multimodal large language models in medicine. *Information Fusion*, 117:102888, 2025. 1

[46] Junshan Xu and Elfar Adalsteinsson. Deformed2self: Self-supervised denoising for dynamic medical imaging. In *International Conference on Medical Image Computing and Computer-Assisted Intervention*, pages 25–35. Springer, 2021. 2

[47] Lijian Xu, Hao Sun, Ziyu Ni, Hongsheng Li, and Shaoting Zhang. Medvilam: A multimodal large language model with advanced generalizability and explainability for med-

ical data understanding and generation. *arXiv preprint arXiv:2409.19684*, 2024. 1

[48] Weiwen Xu, Hou Pong Chan, Long Li, Mahani Aljunied, Ruijing Yuan, Jianyu Wang, Chenghao Xiao, Guizhen Chen, Chaoqun Liu, Zhaodonghui Li, et al. Lingshu: A generalist foundation model for unified multimodal medical understanding and reasoning. *arXiv preprint arXiv:2506.07044*, 2025. 4, 12, 13

[49] Yin Yang, Shuangbin Xu, Yifan Hong, Yantong Cai, Wenli Tang, Jiao Wang, Bairong Shen, Hui Zong, and Guangchuang Yu. Computational modeling for medical data: From data collection to knowledge discovery. *The Innovation Life*, 2(3):100079–1, 2024. 2

[50] Xin Yi, Shunfan Zheng, Linlin Wang, Xiaoling Wang, and Liang He. A safety realignment framework via subspace-oriented model fusion for large language models. *Knowledge-Based Systems*, 306:112701, 2024. 3

[51] Yutong Zhang, Yi Pan, Tianyang Zhong, Peixin Dong, Kangni Xie, Yuxiao Liu, Hanqi Jiang, Zihao Wu, Zhengliang Liu, Wei Zhao, et al. Potential of multimodal large language models for data mining of medical images and free-text reports. *Meta-Radiology*, 2(4):100103, 2024. 1

[52] Can Zhao, Muhan Shao, Aaron Carass, Hao Li, Blake E Dewey, Lotta M Ellingsen, Jonghye Woo, Michael A Guttman, Ari M Blitz, Maureen Stone, et al. Applications of a deep learning method for anti-aliasing and super-resolution in mri. *Magnetic resonance imaging*, 64:132–141, 2019. 3

[53] Yukun Zhao, Lingyong Yan, Weiwei Sun, Guoliang Xing, Shuaiqiang Wang, Chong Meng, Zhicong Cheng, Zhaochun Ren, and Dawei Yin. Improving the robustness of large language models via consistency alignment. *arXiv preprint arXiv:2403.14221*, 2024. 3

[54] Langrui Zhou, Ziteng Zhou, Xinyu Huang, Huiru Wang, Xiangyu Zhang, and Guang Li. Neighboring slice noise2noise: Self-supervised medical image denoising from single noisy image volume. *arXiv preprint arXiv:2411.10831*, 2024. 2

[55] Jinguo Zhu, Weiyun Wang, Zhe Chen, Zhaoyang Liu, Shenglong Ye, Lixin Gu, Hao Tian, Yuchen Duan, Weijie Su, Jie Shao, et al. Internvl3: Exploring advanced training and test-time recipes for open-source multimodal models. *arXiv preprint arXiv:2504.10479*, 2025. 4, 12, 13

[56] Kaijie Zhu, Jindong Wang, Jiaheng Zhou, Zichen Wang, Hao Chen, Yidong Wang, Linyi Yang, Wei Ye, Yue Zhang, Neil Zhenqiang Gong, et al. Promptbench: Towards evaluating the robustness of large language models on adversarial prompts. *arXiv e-prints*, pages arXiv–2306, 2023. 3

Perceive and Calibrate: Analyzing and Enhancing Robustness of Medical Multi-Modal Large Language Models

Supplementary Material

7. OmniMed-based Benchmark

We construct another benchmark based on OmniMed [14] due to its data diversity, which encompasses multiple medical imaging modalities. Similar to the SLAKE-based benchmark mentioned in our main paper, we also construct six different image artifacts across three imaging modalities and 5 different types of language noise, including character-level and sentence-level perturbations. Figure 4 shows the data distribution of the OmniMed-based benchmark, where we select 933/800/948 samples for CT/MRI/X-ray modalities, respectively. It is worth noting that the OmniMed-based benchmark consists exclusively of Multiple-Choice Questions (MCQ), with each question providing four different choices. Therefore, for evaluating model performance on this benchmark, we simply report the accuracy.

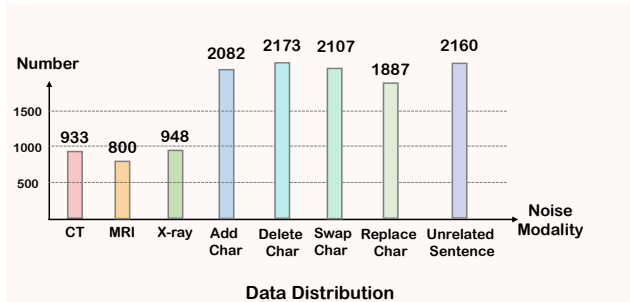


Figure 4. Statistical distribution of modalities and question categories of the OmniMed-based benchmark.

8. Comprehensive Results on SLAKE-based Benchmark

On the SLAKE-based benchmark, we report the performance degradation of two closed-source MLLMs (GPT-5-Mini [35], GPT-4o-Mini [16]) and two closed-source MLLMs (InternVL-3-9B [55] and Lingshu-7B [48]). As demonstrated in Table 6, we notice that MRI aliasing artifacts bring the most severe impact to model performance compared to other imaging noise, which aligns with our observations mentioned in the main paper. The performance degradation under MRI aliasing reaches 26.25%/15.57%/17.21%/35.24% accuracy reduction on closed-ended questions and 21.99%/15.25%/11.47%/22.54% ROUGE score drops on open-ended questions for GPT-5-Mini/GPT-4o-Mini/InternVL/Lingshu, respectively. On the other hand,

X-ray patient movement has minimal impact with no obvious performance decreases on both open-ended and closed-ended questions across the three open-source MLLMs. This phenomenon may arise because X-ray images have higher modal distinctiveness, and minor patient movements cannot significantly distort the essential anatomical structures needed for organ identification and modality classification. These experimental results emphasize that noise in both image and text can affect model performance, which hampers their practical deployment in real-world clinical scenarios.

9. Improvement of IMC Framework on OmniMed-based Benchmark

On the OmniMed-based benchmark, we compare the base MLLM with our proposed denoising framework. Similar to the setting in our main paper, we choose the Qwen2.5-VL-7B as our base model. The experimental results on textual noise are presented in Table 7 while the results on image artifacts are presented across three tables: Table 8 for MRI noise, Table 9 for CT noise, Table 10 for X-ray noise. Specifically, Table 7 demonstrates that our IMC framework can improve prediction accuracy of the base model by 4.14%/4.61%/3.75%/4.03% under randomly delete/add/swap/replace characters, and increases accuracy 5.51% on additional unrelated sentence noise. Tables 8-10 demonstrate that our IMC framework consistently outperforms the base model across all imaging modalities. Specifically, we achieve accuracy improvements of 1.84%/4.30%/3.06% for MRI artifacts (human motion/aliasing/banding), 2.47%/0.99% for CT artifacts (low dose/sparse view), and 2.35% for X-ray patient movement, respectively.

10. Case Study

We visualize some cases in this section for demonstrating the effectiveness of our proposed denoising framework. Figure 5 presents the close-ended and open-ended questions on SLAKE-based benchmark perturbed by CT low dose artifact. And the multiple-choice question on OmniMed-based MRI motion noise. fact. The base model initially generates correct responses. However, when encountering CT low-dose noise, the model produces incorrect results. After applying our method to calibrate the image latent features, the model is able to generate correct answers again.

Table 6. The experiments carried out on SLAKE-based benchmark, which shows the performance comparison of open-source and closed-source MLLMs robustness across six medical imaging artifacts and five textual noise types. Subscripts denote performance drops.

MLLMs	Modality	Noise	ACC(↑)	ROUGE(↑)	BLEU(↑)	Recall(↑)
GPT-5-Mini [35]	MRI	MRI Original	80.33	45.79	7.37	48.10
		MRI Human Motion	72.13 _{-8.20}	45.53 _{-0.26}	7.32 _{-0.05}	46.12 _{-1.98}
		MRI Aliasing	54.10 _{-26.23}	23.80 _{-21.99}	3.31 _{-4.06}	20.80 _{-27.30}
		MRI Banding	72.95 _{-7.38}	45.11 _{-0.68}	7.54 _{+0.17}	45.33 _{-2.77}
	CT	CT Original	79.64	49.23	7.68	45.18
		CT Sparse View	78.21 _{-1.43}	42.79 _{-6.44}	6.19 _{-1.49}	36.89 _{-8.29}
		CT Low Dose	79.29 _{-0.35}	48.72 _{-0.51}	7.54 _{-0.14}	44.86 _{-0.32}
	X-ray	X-ray Original	68.57	46.98	6.68	40.49
		X-ray Patient Movement	66.43 _{-2.14}	46.67 _{-0.31}	6.53 _{-0.15}	39.96 _{-0.53}
GPT-4o-Mini [16]	MRI	MRI Original	74.59	38.89	5.73	36.82
		MRI Human Motion	70.49 _{-4.10}	28.17 _{-10.72}	4.41 _{-1.32}	26.98 _{-9.84}
		MRI Aliasing	59.02 _{-15.57}	23.64 _{-15.25}	3.56 _{-2.17}	21.85 _{-14.97}
		MRI Banding	74.59 _{-0.00}	35.50 _{-3.39}	5.22 _{-0.51}	33.80 _{-3.02}
	CT	CT Original	70.71	34.78	5.40	33.02
		CT Sparse View	65.71 _{-5.00}	29.11 _{-5.67}	4.87 _{-0.53}	29.10 _{-3.92}
		CT Low Dose	67.86 _{-2.85}	27.91 _{-6.87}	4.15 _{-1.25}	26.05 _{-6.97}
	X-ray	X-ray Original	77.86	47.33	5.41	33.83
		X-ray Patient Movement	72.14 _{-5.72}	42.48 _{-4.85}	4.65 _{-0.76}	29.33 _{-4.50}
InternVL-3-9B [55]	MRI	MRI Original	77.05	43.09	7.37	44.26
		MRI Human Motion	71.31 _{-5.74}	38.21 _{-4.88}	6.44 _{-0.93}	39.57 _{-4.69}
		MRI Aliasing	59.84 _{-17.21}	31.62 _{-11.47}	4.97 _{-2.40}	31.69 _{-12.57}
		MRI Banding	74.59 _{-2.46}	42.34 _{-0.75}	6.60 _{-0.77}	42.73 _{-1.53}
		Character Noise	65.57 _{-11.48}	33.33 _{-9.76}	5.54 _{-1.83}	37.02 _{-7.24}
		Sentence Noise	67.21 _{-9.84}	29.70 _{-13.39}	4.34 _{-3.03}	33.10 _{-11.16}
	CT	CT Original	78.57	37.68	6.61	40.23
		CT Sparse View	67.86 _{-10.71}	24.90 _{-12.78}	4.06 _{-2.55}	25.89 _{-14.34}
		CT Low Dose	71.43 _{-7.14}	36.65 _{-1.03}	6.53 _{-0.08}	38.47 _{-1.76}
		Character Noise	62.86 _{-15.71}	24.42 _{-13.26}	3.90 _{-2.71}	28.50 _{-11.73}
	X-ray	Sentence Noise	68.93 _{-9.64}	24.00 _{-13.68}	3.64 _{-2.97}	27.06 _{-13.17}
		X-ray Original	72.14	37.08	5.62	40.56
		X-ray Patient Movement	72.86 _{+0.72}	35.25 _{-1.83}	4.91 _{-0.71}	39.17 _{-1.39}
		Character Noise	65.71 _{-6.43}	23.58 _{-13.50}	3.34 _{-2.28}	32.17 _{-8.39}
		Sentence Noise	61.43 _{-10.71}	22.06 _{-15.02}	1.75 _{-3.87}	30.35 _{-10.21}
Lingshu-7B [48]	MRI	MRI Original	91.80	86.47	8.49	14.25
		MRI Human Motion	84.43 _{-7.37}	82.02 _{-4.45}	8.35 _{-0.14}	14.77 _{+0.52}
		MRI Aliasing	56.56 _{-35.24}	63.93 _{-22.54}	6.96 _{-1.53}	12.92 _{-1.33}
		MRI Banding	88.52 _{-3.28}	83.40 _{-3.07}	7.10 _{-1.39}	12.65 _{-1.60}
		Character Noise	76.23 _{-15.57}	77.75 _{-8.72}	7.56 _{-0.93}	12.88 _{-1.37}
		Sentence Noise	81.97 _{-9.83}	83.37 _{-3.10}	8.98 _{+0.49}	15.34 _{+1.09}
	CT	CT Original	78.57	75.10	3.26	10.87
		CT Sparse View	77.14 _{-1.43}	59.78 _{-15.32}	2.33 _{-0.93}	7.95 _{-2.92}
		CT Low Dose	75.71 _{-2.86}	70.56 _{-4.54}	2.81 _{-0.45}	9.27 _{-1.60}
		Character Noise	69.29 _{-9.28}	63.42 _{-11.68}	2.51 _{-0.75}	8.45 _{-2.42}
	X-ray	Sentence Noise	74.64 _{-3.93}	68.69 _{-6.41}	2.85 _{-0.41}	9.52 _{-1.35}
		X-ray Original	82.14	82.17	4.19	11.86
		X-ray Patient Movement	82.14 _{+0.00}	76.97 _{-5.20}	3.53 _{-0.66}	10.11 _{-1.75}
		Character Noise	77.14 _{-5.00}	66.29 _{-15.88}	3.33 _{-0.86}	11.20 _{-0.66}
		Sentence Noise	73.57 _{-8.57}	75.37 _{-6.80}	3.43 _{-0.76}	11.32 _{-0.54}

Table 7. The experiments carried out on OmniMed-based benchmark, which shows the performance comparison of the robustness of based model and our method across five textual noise types. Subscripts denote performance drops.

Data & Model	Text Noise				
	Delete Characters	Add Characters	Swap Characters	Replace Characters	Unrelated Sentences
Original Data with Base Model	63.41	64.02	62.98	64.71	63.70
Noisy Data with Base Model	58.49 _{-4.92}	58.98 _{-5.04}	58.14 _{-4.84}	59.67 _{-5.04}	57.64 _{-6.06}
Noisy Data with Our Approach	62.63 _{-0.78}	63.59 _{-0.43}	61.89 _{-1.09}	63.70 _{-1.01}	63.15 _{-0.55}

Table 8. The experiments carried out on OmniMed-based benchmark, which shows the performance comparison of the robustness of based model and our method across three MRI artifacts. Subscripts denote performance drops.

MRI						
Original	Human Motion		Aliasing		Banding	
	Base Model	Ours	Base Model	Ours	Base Model	Ours
73.62	68.71 _{-4.91}	70.55 _{-3.07}	48.77 _{-24.85}	53.07 _{-20.55}	69.33 _{-4.29}	72.39 _{-1.23}

Table 9. The experiments carried out on OmniMed-based benchmark, which shows the performance comparison of the robustness of based model and our method across two CT artifacts. Subscripts denote performance drops.

CT				
Original	Low Dose		Sparse View	
	Base Model	Ours	Base Model	Ours
54.68	43.10 _{-11.58}	45.57 _{-9.11}	47.78 _{-6.90}	48.77 _{-5.91}

Table 10. The experiments carried out on OmniMed-based benchmark, which shows the performance comparison of the robustness of based model and our method on X-ray artifacts. Subscripts denote performance drops.

X-ray		
Original	Patient Movement	
	Base Model	Ours
78.35	72.24 _{-6.11}	74.59 _{-3.76}

11. Prompts Used for Constructing Agents

In this section, we illustrate the prompts used for constructing agents for textual noise removal. Figure 6 shows the prompt for building the *Classifier and Denoiser* that identifies and removes character-level and sentence-level noise. Figure 7 shows the prompt for the *Residual Noise Checker* that verifies whether the denoised result still contains residual noise. Figure 8 shows the prompt for the *Optimal Result Selector* that selects the most accurate denoised sentence from multiple candidates. Figure 9 shows the prompt for the *Output Validator* that ensures the denoised sentence is noise-free and contextually consistent.

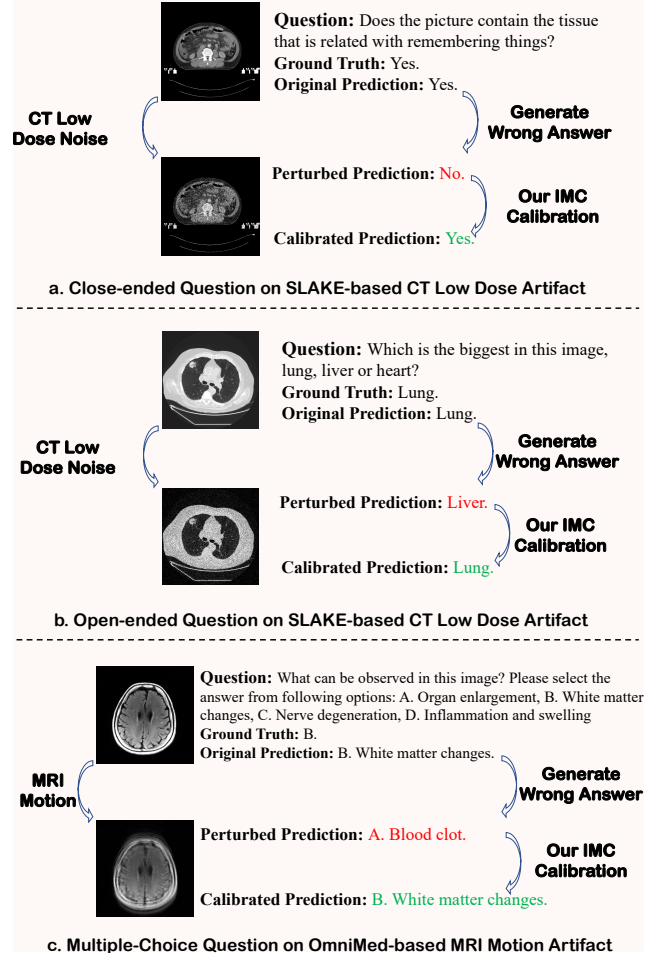


Figure 5. (a-b) Case studies of close-ended and open-ended questions on SLAKE-based CT low dose artifact; (c) Case study of Multiple-Choice Question on OmniMed-based MRI Motion noise.

Prompting MLLMs to Construct the Classifier and Denoiser

"I will provide you with a sentence containing character-level or sentence-level errors. Your task is to identify these errors and reply with the corrected version of the sentence.

The noise occurs at the character level and can include the following types:

- Randomly added characters: Additional characters are inserted randomly.
- Random character substitution: Some characters are replaced with incorrect ones.
- Random character swaps: The order of some characters is shuffled.
- Randomly deleted characters: Some characters are removed from the sentence.

The noise occurs at the sentence level and includes the following type:

-Additional noisy sentences: Extra unrelated sentences are inserted before or after the main medical-related question sentence. These unrelated sentences may discuss non-medical topics or provide irrelevant information, and they must be removed. For example: Input: The Pacific Ocean is the largest ocean on Earth. What modality is used to take this image? The sentence 'The Pacific Ocean is the largest ocean on Earth' is unrelated to medical topics and should be removed. The final corrected output is: What modality is used to take this image?

Rules: Always retain the main question sentence related to medical topics. Remove all sentences that are irrelevant or unrelated to the medical question.

The corrected output should only include the medical question sentence, with no additional words or unrelated content.

The input is: " + **Original_Question** + "Your output should only contain the corrected sentence with no other words."

Figure 6. Message used to prompt the base MLLM to construct the first agent (i.e., *Classifier and Denoiser*) that identifies noise types and performs corresponding noise removal operations. The bold font **Original_Question** represents the noisy question input for denoising.

Prompting MLLMs to Construct the Residual Noise Checker

"I will provide you with a sentence that may or may not contain character-level or sentence-level noise. Your task is to determine if the sentence contains such noise.

Character-level noise can include:

1. Randomly added characters: Additional characters are inserted randomly.
2. Random character substitution: Some characters are replaced with incorrect ones.
3. Random character swaps: The order of some characters is shuffled.
4. Randomly deleted characters: Some characters are removed from the sentence.

Sentence-level noise: The input contains one medical-related sentence and one non-medical-related sentence.

Your task is to identify and remove the non-medical-related sentence, keeping only the medical-related sentence.

The sentence is: " + **Possible_Prediction_Result** + "Your output should only be one of the following:

'Yes' (if the sentence contains character-level or sentence-level noise).

'No' (if the sentence does not contain character-level or sentence-level noise)."

Figure 7. Message used to prompt the base MLLM to construct the second agent (i.e., *Residual Noise Checker*) that determines whether the denoised results from previous step still contain noise. The bold font **Possible_Prediction_Result** represents the denoised result outputted from the previous agent *Classifier and Denoiser*.

Prompting MLLMs to Construct the Optimal Result Selector

"I will provide you with a list of sentences and a noisy sentence as a reference. Your task is to evaluate these sentences and select the one that is most likely to be the original, normal version of the noisy sentence. You should make this judgment based on two factors:

1. Majority of the normal sentence: Select the sentence that appears most frequently.
2. Relevance to the image information: Evaluate how well each sentence aligns with the information provided about the input image. Sentences that are more relevant to the image description should be preferred.

Your Task: Now, evaluate the following sentences and select the one that is most likely to be the original, normal sentence.

Noisy sentence: "**Original_Question**" Sentences to evaluate: **{Possible_Prediction_Results}**

Your output should contain only the selected sentence no other words."

Figure 8. Message used to prompt the base MLLM to construct the third agent (i.e., *Optimal Result Selector*). This agent compares results from k parallel micro loops to identify the output that is most noise-free compared to the input sentence and consistent with the visual information. The bold font **Original_Question** represents the input noisy sentence in this round, and **{Possible_Prediction_Results}** means the collection of k outputs from previous micro loops.

Prompting MLLMs to Construct the Output Validator

"You will be given:

1. Original Sentence (with noise): A sentence containing character-level or sentence-level noise: Character-level noise: Randomly added, substituted, swapped, or deleted characters. Sentence-level noise: Additional unrelated sentences before or after the main sentence.
2. Denoised Sentence (output): A processed version meant to remove the noise.

Your task is to determine if the Denoised Sentence is a valid, noise-free version of the Original Sentence by checking:

1. Does it have almost the same structure with the Original Sentence and the content is related to the provided medical image?
2. Is it free of all character-level and sentence-level noise?

The original sentence is: " + **Original_Question** + " The denoised sentence is: " + **Selected_Result** + "

Your output should only be one of the following:

'Yes' (if the denoised sentence is accurate and noise-free).

'No' (if it is inaccurate.)"

Figure 9. Message used to prompt the base MLLM to construct the last agent (i.e., *Output Validator*) that determines whether the result is a coherent and logically consistent sentence. The bold font **Original_Question** represents the input noisy sentence in this round, and **{Possible_Prediction_Results}** means the collection of k outputs from previous micro loops.